Measurement of the Lifetime of B-Hadrons and a Determination of $|V_{cb}|$

The L3 Collaboration

ABSTRACT

From a fit to the impact parameter distribution of lepton tracks from semileptonic b decay, the lifetime of B-hadrons produced in e^+e^- collisions at the Z^0 is measured to be 1.32 ± 0.08 (stat.) $\pm$ 0.09 (sys.) ps. Combined with an earlier measurement of the branching ratio $\mathrm{Br}(B \to \ell\nu X)$, the CKM matrix element $|V_{cb}|$ is determined to be 0.046 ± 0.002 (exp.) $^{+0.004}_{-0.003}$ (theory).

L3 Preprint #32
July 3, 1991

Introduction

In the Standard Model [1], the dominant decay of hadrons containing a b-quark proceeds through a flavour-changing transition from the b-quark to a c- or u-quark, with a strength described by the elements V_{cb} and V_{ub} of the CKM matrix [2]. Thus, a measurement of the lifetime of B-hadrons constrains these matrix elements, which are fundamental parameters of the Standard Model. The B-hadron lifetime has been measured by experiments at PEP and PETRA [3] and, more recently, at LEP [4]. The lifetime can be measured with higher precision at LEP than in the e^+e^- continuum because of the larger production rate of b-quarks at the Z^0 resonance and the lower background from the lighter quarks, especially the charm quark.

We determine the lifetime of B-hadrons from a maximum likelihood fit to the impact parameter distribution of the inclusive leptons from semileptonic b decays. As in our earlier publications [5-7], leptons with large momentum and large transverse momentum with respect to the nearest jet are used to tag semileptonic b decays. Since the B-hadrons are not fully reconstructed in this analysis, we measure the average lifetime of B-hadrons, weighted by their production rates in the Z^0 decay and by their semileptonic branching ratios. Measurements at lower center-of-mass energies [8] indicate that the lifetime difference between the B^0- and B^+-mesons is small. This is in agreement with the prediction of the spectator model [9].

Inclusive muon and electron events are selected from a sample of about 115,000 $e^+e^- \rightarrow \textit{hadrons}$ events, recorded in 1990 with the L3 detector at $\sqrt{s} \approx M_Z$. The data sample corresponds to an integrated luminosity of 5.5 pb^{-1}.

The L3 detector

The detector consists of a central tracking chamber, a high resolution electromagnetic calorimeter composed of BGO crystals, a ring of scintillation counters, a uranium and brass hadron calorimeter with proportional wire chamber readout, and a precise muon spectrometer. These detectors are installed in a 12 m diameter solenoid which provides a uniform field of 0.5 T along the beam direction. A detailed description of the L3 detector is given in reference [10].

The central tracking chamber is a time expansion chamber (TEC) which consists of two cylinders, the inner and outer chambers, with 12 and 24 sectors, respectively. The R-ϕ coordinate of a track is measured with a maximum of 62 anode wires (8 in the inner chamber, 54 in the outer). The chamber is separated from the beam line by two concentric beryllium tubes with a total thickness of 1.5 mm. The first spatial coordinate is measured at a distance of 110 mm from the beam line, and the last one at a distance of 427 mm. The single wire resolution is 58 μm averaged over the entire cell and the double-track resolution is 640 μm.

The fine segmentation of the BGO detector and the hadron calorimeter allows us to measure the direction of jets with an angular resolution of 2.1°, and to measure the total energy of hadronic events from Z^0 decay with a resolution of 10.2% [11]. The muon detector consists of three layers of precise drift chambers, which measure a muon trajectory 56 times in the bending plane, and 8 times in the non-bending direction. Data used in this analysis covered the following ranges of polar angles:

- Central tracking chamber: $41° < \theta < 139°$,

- Electromagnetic calorimeter: $42° < \theta < 138°$,
- Hadron calorimeter: $5° < \theta < 175°$,
- Muon chambers: $36° < \theta < 144°$.

Event selection

The trigger requirements and the selection criteria for hadronic events containing electrons and muons have been described earlier [7]. For this analysis, additional requirements are used to ensure that the lepton track is well measured in the TEC. A minimum of 40 hits is required on the track, and at least 5 of them must be from the inner TEC. The track must also include at least one hit from the three innermost wires, and the distance of closest approach to the interaction point must be less than 5 mm in the $R-\phi$ projection. The spatial resolution in the TEC is worse for hits close to the anode or cathode wires. Therefore, we exclude tracks which are within 10 mrad of either the anode or cathode planes. Only well-reconstructed tracks are kept by requiring that the χ^2 probability of the track fit is larger than 2%.

For muons, in addition to the standard cuts, we use a χ^2 method to match a TEC track in momentum and direction with the corresponding muon chamber track. The effects of multiple scattering and energy loss in the calorimeters are taken into account in the matching. The track in the central tracking chamber corresponding to the best χ^2 value below a maximum limit is considered to be the muon candidate.

Because of the hard fragmentation and large mass of the b-quark, leptons from semileptonic B-hadron decay have a large momentum and a large transverse momentum with respect to the b-quark direction. Therefore, by cutting on these quantities we preferentially select $Z^0 \to b\bar{b}$ events. Only muons and electrons with momenta greater than 4 GeV are used in this analysis. The transverse momentum, $p_\perp$, calculated with respect to the nearest jet axis is required to exceed 1.5 GeV for muons and 1 GeV for electrons, and is required to be less than 6 GeV. The lepton is excluded from the calculation of the jet direction. If there is no jet with an energy greater than 6 GeV in the same hemisphere as the lepton, $p_\perp$ is calculated relative to the thrust axis of the event.

After all cuts, we are left with 1386 inclusive lepton candidates. These include 673 electron candidates and 713 muon candidates. No tracks originating from K^0 or Λ decay have been found in the lepton candidate sample. This was established by studying the invariant-mass distribution of the lepton candidates with all other oppositely charged tracks which are consistent with coming from a common secondary vertex. Monte Carlo simulations also show no contamination from K^0 or Λ decay products in the lepton sample.

Lepton classification

We classify the inclusive lepton events into the following categories (and their charge conjugate reactions),

1) Prompt $b \to \ell$;
2) Cascade $b \to c \to \ell$ including $b \to c + \bar{c} + s$ where $\bar{c} \to \ell$, and $b \to \tau \to \ell$;
3) Prompt $c \to \ell$;

4) Background from decays: $\pi, K \to \ell$;
5) Background from hadrons misidentified as leptons.

For each category, we generate Monte Carlo events using the parton shower program JETSET 7.2 [12]. The events are passed through the L3 detector simulation [13], which includes the effects of experimental resolution, energy loss, multiple scattering, interactions, and decays in the detector materials. The events are generated with the parameter $\Lambda_{\rm LL} = 290$ MeV and string fragmentation. The Peterson fragmentation function [14] is used in the Monte Carlo simulation to describe the fragmentation of c- and b-quarks. The input fragmentation parameters used in the generator are $\epsilon_c^z = 0.07$ for charm quarks, found by extrapolation from PETRA and PEP data [15], and $\epsilon_b^z = 0.008$ for bottom quarks, taken from our own measurement [7]. We also use the L3 measurement of $\mathrm{Br}(B \to \ell\nu X) = 0.119 \pm 0.003\,(\mathrm{stat.}) \pm 0.006\,(\mathrm{sys.})$ [7] and take $\mathrm{Br}(D \to \ell\nu X) = 0.096 \pm 0.006\,(\mathrm{stat.} + \mathrm{sys.})$ from measurements at PETRA and PEP [16].

The p and $p_\perp$ spectra for the inclusive leptons are well reproduced by the Monte Carlo simulation, as shown in previous publications [5-7]. The prompt b-decay contribution dominates at large transverse lepton momentum. The Monte Carlo estimates for the fraction of each lepton category after all cuts are given in Table 1.

Category	muons	electrons
1: prompt $b \to \ell$	82.1%	84.4%
2: cascade ℓ	5.3%	4.3%
3: prompt $c \to \ell$	4.5%	1.7%
4: decay $\pi, K \to \ell$	1.2%	0.2%
5: misid. hadrons	6.9%	9.4%

Table 1: Monte Carlo estimates of the fraction of each lepton category in the data, after application of the cuts described in the text.

Impact parameter method

The B-hadron lifetime is determined from a measurement of the signed impact parameter of the selected lepton candidate tracks. The impact parameter is defined as the distance of closest approach of the lepton track to the estimated primary production vertex. We use the projected impact parameter, δ, in the plane transverse to the beam ($R - \phi$ projection), because the beam size is smaller and the spatial resolution of the tracking chamber is better in this plane than along the beam axis. An advantage of the impact parameter method is that the measured lifetime is not sensitive to the B-hadron momentum and hence to a precise knowledge of the b-quark fragmentation parameters. The B-hadron direction is approximated by the event thrust axis. The impact parameter is taken to be positive if the lepton

track intersects with the event thrust axis in the apparent flight direction of the B-hadron, and is taken to be negative if it intersects opposite to this direction. The negative values are a consequence of the experimental resolution and of the approximation of the B-hadron direction by the event thrust axis. Uncertainties in the measurement of the impact parameter can result from the following sources:

(1) the uncertainty on the position of the primary vertex,
(2) the error from the track reconstruction,
(3) the multiple scattering in the beryllium tubes.

Since the e^+e^- collision point is not known on an event-by-event basis, the average position is taken to be the primary vertex. It is determined for each LEP fill from good quality tracks in hadronic events with a statistical precision of a few microns. From the variation in the measurement of the beam position within a LEP fill, which includes the effects of changes in the beam steering, we estimate an upper limit of 36 μm on the systematic error of the beam position determination.

The experimental resolution in δ and the size of the beam spot are found using high momentum tracks in the reactions $e^+e^- \rightarrow e^+e^-$ and $e^+e^- \rightarrow \mu^+\mu^-$. The resolution is determined by measuring the distance, d, in the $R-\phi$ plane between the two tracks at the primary vertex. From the r.m.s. of this distribution, σ_d, we obtain the average experimental resolution in the distance of closest approach, $< \sigma_{exp} > = \sigma_d/\sqrt{2} = 144 \pm 1$ μm for particle momenta of ≈ 45 GeV, where the error is statistical only.

For a given azimuthal angle, the width of the impact parameter distribution of tracks originating from the primary vertex measures the projected size of the beam spot, folded with the resolution in δ. Subtracting in quadrature $< \sigma_{exp} >$ from the r.m.s. of the δ distribution, we determine an r.m.s. beam spot size of $\sigma_x = 196 \pm 5$ μm in the horizontal direction and $\sigma_y = 24 \pm 25$ μm in the vertical direction. The determination of the B-hadron lifetime is relatively insensitive to the exact value of the beam spot size, as shown below in the study of the systematic error.

For lower momentum tracks, a small additional contribution from multiple scattering in the beryllium tubes must be taken into account. This can be parametrized as a function of the track momentum p by $\sigma_{mult} = 83$ μm$/p$ [GeV].

The total error on the measured distance of closest approach, σ_δ, can then be written as:

$$\sigma_\delta^2 = \sigma_{exp}^2 + \sigma_{mult}^2 + \sigma_x^2 sin^2\phi + \sigma_y^2 cos^2\phi, \qquad (1)$$

where ϕ is the azimuthal angle of the track. The experimental error, σ_{exp}, is taken from the covariance matrix of the track fit for each lepton candidate.

We determine the lifetime of B-hadrons, τ_B, using a binned maximum likelihood fit to the measured impact parameter distribution, taking into account the expected contributions of the lepton categories mentioned above. The impact parameter distributions for the prompt and cascade lepton sources depend on the lifetime of the parent hadrons. It is through this dependence that the B-hadron lifetime is measured. The impact parameter distributions for the five lepton sources are obtained from the data or from Monte Carlo simulations, as described in the next two sections.

Prompt and cascade leptons

The impact parameter distributions for the prompt and cascade leptons can be expressed as a convolution of two functions: the true impact parameter distribution, which depends on the lifetime of the B- or D-hadrons, and the resolution function, which describes the smearing of δ due to the finite resolution.

The true impact parameter distributions have been determined from Monte Carlo simulations using inclusive leptons which satisfy the selection criteria described above. The true impact parameter, δ_t, is calculated relative to the event production vertex, as generated in the Monte Carlo simulation. The sign of δ_t is chosen using the reconstructed event thrust axis, in order to take into account the uncertainty of approximating the B-hadron direction by the event thrust axis.

For prompt $b \to \ell$ leptons, the true impact parameter distribution scales with $\delta_t/c\tau_B$. It has been determined from the Monte Carlo simulation using $\tau_B = 1.31$ ps, and it is scaled for other τ_B values in the fit. For the cascade leptons, the impact parameter depends on both the B- and D-hadron (or τ-lepton) lifetimes. However, it is dominated by the lifetime of the initial B-hadron, and we also use $\tau_B = 1.31$ ps as the scaling lifetime for this lepton category. For prompt $c \to l$, an average value of $\tau_D = 0.68$ ps is used as the scaling lifetime. This value has been estimated from the lifetimes of the various charmed particles, weighted by their relative production rates and semileptonic branching ratios. As discussed later, the determination of the B-hadron lifetime is insensitive to the value of τ_D used in the fit. The various true impact parameter distributions are determined separately for muons and electrons. We perform a fit to the Monte Carlo generated distributions using two exponential functions for each of the regions $\delta < 0$ and $\delta > 0$, and use this parametrization in the likelihood fit. Typical values of the mean true impact parameter from the Monte Carlo events are 175 μm, 203 μm, and 47 μm for $b \to \ell$, cascade and $c \to \ell$ leptons, respectively.

The experimental impact parameter resolution function is determined by using hadronic tracks in the data which meet all selection criteria applied to the lepton candidates, except the lepton identification and the $p_\perp$ cuts. Furthermore, we select only those tracks whose flight directions are nearly parallel to the thrust axis in the $R - \phi$ projection by requiring $|\sin\Delta\phi| < 0.02$, where $\Delta\phi$ is the difference in azimuthal angle between the track momentum vector and the event thrust axis. Due to this requirement, the impact parameter measurement is dominated by the experimental resolution.

We obtained the resolution function by measuring $\delta/\overline{\sigma}_\delta$ for the hadronic tracks. The parameter $\overline{\sigma}_\delta = 216$ μm is the average of the impact parameter errors, found using equation (1). The resulting scaled impact parameter distribution $\delta/\overline{\sigma}_\delta$ for the hadronic tracks is shown in Figure 1(a). Residual lifetime effects cause the small excess on the positive side of the distribution. Therefore, a fit using the sum of two Gaussians is performed only over the negative side of the distribution. The curve in Figure 1(a) shows the result of the fit over the entire distribution. The central region of the distribution is well described by a Gaussian of width 1.09 ± 0.11. A second Gaussian, of width 2.2 ± 0.6 and fractional amplitude 10%, is needed to describe the small tails due to overlapping tracks. From these studies, we parametrize the impact parameter resolution function as the sum of two Gaussians having widths

of $1.09\overline{\sigma}_\delta$ and $2.2\overline{\sigma}_\delta$, respectively,

Further studies using large-angle $e^+e^- \rightarrow e^+e^-$ events have been performed to check whether the assignment of the measurement error according to equation (1) is correct. The result of this test is shown in Figure 1(b), where the distribution of δ/σ_δ is shown for tracks from $e^+e^- \rightarrow e^+e^-$ events. In this case, the sign of δ is determined by whether or not the primary vertex is inside the circle formed by the track fit. The distribution is well described by a Gaussian of width 1.06 ± 0.01, where the error is statistical only. This is shown by the curve in Figure 1(b). This result is in good agreement with the impact parameter distribution of the hadronic tracks in Figure 1(a), and shows that the measurement error on the impact parameter is well understood.

Background and π, K decay leptons

The impact parameter distribution for misidentified hadrons is determined from the δ-distribution of hadron tracks in the data which fulfill all the selection criteria, but fail the lepton identification. The resulting impact parameter distribution is shown in Figure 2. The distribution has a mean value of 57 ± 5 μm, which is in good agreement with the expectation from the Monte Carlo simulation. A fit is made to this distribution using three Gaussians functions, having widths of $\sigma_\delta = 222$ μm, 414 μm, and 2.2 mm, respectively. The widths of the first two Gaussians agree with the values found earlier for the width of the resolution function. The third Gaussian describes the tails of the distribution, which are caused by hadron tracks from decays of long lived particles.

Due to the relatively small radius of the central tracking chamber, the contribution of background from π and K decay in the selected data sample is only at the 1% level. Decays in flight can generate large impact parameters due to the kink in the reconstructed track. Therefore, the impact parameter distribution from this source is wider than for the other lepton categories. A sample of tracks which originate from the decays of π and K and meet the selection criteria are selected from the Monte Carlo events. A fit is made to their impact parameter distribution using the sum of a Gaussian and an exponential function. This parametrization is used in the fit for the decay distribution.

Maximum likelihood fit

The B-hadron lifetime, τ_B, is determined from a binned maximum likelihood fit to the impact parameter distribution. The probability in each bin is determined from the measured and the expected number of events in this bin using Poisson statistics. The measured impact parameter distribution is shown in Figure 3. The preponderance of positive values, as seen from the measured mean of 176 ± 20 μm, is due to the lifetime of the B-hadrons. The expected impact parameter distribution, which depends on τ_B, is the sum of the δ-distributions of the five lepton categories, weighted by the fractions as given in Table 1. The fit is performed simultaneously for the muon and electron δ-distributions over the range $|\delta| < 3$ mm, using a bin size of 0.2 mm. The result of the fit is $\tau_B = 1.32 \pm 0.08$ ps, where the error is statistical only. The expected impact parameter distribution for this value of τ_B is shown in Figure 3 as a solid line, in good agreement with the measurement. The

calculated χ^2 per degree of freedom is 54/59. The contributions from the different lepton sources are also shown in the figure.

Checks and systematic errors

We have performed several consistency checks to verify the analysis and the fitting procedures. As a necessary check of the method, Monte Carlo events were generated with various input B-hadron lifetimes over a range from 0.5 to 1.5 ps. The events are analyzed in the same manner as the data. The measured B-hadron lifetime obtained for each sample is found to be in good agreement with the input lifetime. For example, using Monte Carlo events generated with an input B-hadron lifetime of 1.31 ps, we obtain a value of 1.33 ± 0.03 ps.

To check for biases, we also repeat the analysis for different subsets of the data. The average B-hadron lifetimes obtained for these different event samples are listed in Table 2. We determine the lifetime separately for electrons and muons, for positively and negatively charged leptons, and for leptons in the region where the effect of the beam spot size is smaller, namely horizontally-produced leptons where the azimuthal angle satisfies $|\sin\phi| < 0.5$. As a further check, we measure the lifetime for a sample selected with a lower cut on the transverse momentum of the lepton relative to the nearest jet axis, $p_\perp > 0.5$ GeV for electrons and $p_\perp > 1.0$ GeV for muons. Finally, we repeat the analysis using only events with $|\delta| < 1.5$ mm. Within the statistical errors, all the results are compatible with each other.

Event Sample	N_{events}	τ_B (ps)
standard	1386	1.32 ± 0.08
muons	713	1.35 ± 0.11
electrons	673	1.29 ± 0.11
negative leptons	715	1.37 ± 0.11
positive leptons	671	1.25 ± 0.11
$\|\sin\phi\| < 0.5$	416	1.26 ± 0.13
lower $p_\perp$ cut	1843	1.33 ± 0.07
$\|\delta\| < 1.5$ mm	1364	1.29 ± 0.08

Table 2: Measurements of the B-hadron lifetime for different event samples.

Table 3 contains the various contributions to the systematic error in the lifetime measurement. We estimate each contribution by changing the corresponding parameters by one standard deviation or more of their known (or estimated) uncertainties and by repeating the lifetime analysis with the new values. The error on the fragmentation parameter, ϵ_b, is taken from our previous measurement [7]. The error due to the uncertainty in the average charm hadron lifetime τ_D is determined by varying this value over a range of ± 0.2 ps, to compensate for the lifetime difference

between the D^+- and D^0-mesons. We have varied the fraction of prompt $b \to \ell$ in the fit by $\pm 20\%$, scaling the other lepton sources proportionally according to their fractions. We estimate the uncertainties from the parametrizations of the prompt and cascade true impact parameter distributions by changing the parameters used in the corresponding functions by their associated errors. The largest error comes from the uncertainty in the parametrization of the prompt $b \to \ell$ decays, since they are the dominant contribution in the event sample. The uncertainty in the parametrization of the hadronic background is estimated by using different track selection criteria.

Contribution	$\Delta\tau_B$ (ps)
changing the b fragmentation parameter ϵ_b by its error	0.001
changing the average τ_D by ± 0.2 ps	0.01
variation of prompt lepton source fraction by $\pm 20\%$	0.02
variation of true impact parameter distribution for $b \to \ell$	0.05
variation of true impact parameter distribution for cascades	0.02
variation of true impact parameter distribution for $c \to \ell$	0.01
variation of the shape of the hadronic background	0.03
changing the width of the resolution function	0.04
changing the tracking chamber drift velocity	0.03
changing the tracking chamber zero time	0.04
changing the beam spot size by 50 μm	0.01
shifting the beam spot position by 50 μm	0.013
changing the bin width and edge	0.005

Table 3: Systematic uncertainties in the B-hadron lifetime measurement.

The systematic error due to the uncertainty in the impact parameter resolution function is determined by changing the value of $\overline{\sigma}_\delta$ by $\pm 10\%$ and varying the amount of the larger-width Gaussian used in describing the resolution function. Systematic shifts in the impact parameter measurement can arise from errors in the calibration of the central tracking chamber. The crucial calibration parameters are the drift velocity and the zero time of the drift-time measurement. We determine the systematic errors from these sources by repeating the lifetime analysis using drift velocity and zero time values obtained from different calibration procedures. Similarly, the analysis is repeated by varying both the beam spot size and average position by 50 μm. The systematic error due to the binning in the likelihood fit is estimated by repeating the analysis with different bin widths and edges.

Adding the various contributions in quadrature, the total systematic error on τ_B is estimated to be 0.09 ps. Thus, the B-hadron lifetime is determined to be:

$$\tau_B = 1.32 \pm 0.08 \text{ (stat.)} \pm 0.09 \text{ (sys.) ps.}$$

This value is in good agreement with other measurements at LEP [4], PEP and PETRA [3].

Determination of $|V_{cb}|$

This measurement of the B-hadron lifetime, combined with our previous measurement [7] of the semileptonic branching ratio, $\text{Br}(B \to \ell\nu X) = 0.119 \pm 0.003 \pm 0.006$, can be used to determine the magnitude of the CKM matrix element $|V_{cb}|$. The semileptonic decay width of B-hadrons, which is obtained from the semileptonic branching ratio and the lifetime, is related to the CKM matrix elements by [17]:

$$\Gamma(B \to \ell\nu X) = \frac{Br(B \to \ell\nu X)}{\tau_B} = \frac{G_F^2 m_b^5}{192\pi^3} \; (f_c \; |V_{cb}|^2 + f_u \; |V_{ub}|^2). \qquad (2)$$

The parameters $f_q (q = u, c)$ account for quark-mass effects and QCD corrections, and can be approximated by [18]:

$$f_q \simeq (1 - 8\epsilon_q^2 + 8\epsilon_q^6 - \epsilon_q^8 - 24\epsilon_q^4 \ln \epsilon_q) \; (1 - \frac{2}{3}\frac{\alpha_s(m_b^2)}{\pi}[(\pi^2 - \frac{31}{4})(1 - \epsilon_q)^2 + \frac{3}{2}]),$$

where $\epsilon_q = m_q/m_b$.

To calculate f_c and f_u, we use the following quark mass values, which were obtained by the ARGUS Collaboration in the framework of the ACCMM model [19] from a fit to the lepton momentum spectrum in semileptonic B-meson decays [21]: $m_b = 4.95 \pm 0.07 \; GeV$ and $m_b - m_c = 3.30 \pm 0.02 \; GeV$. In order to include uncertainties in the model, we increase the error on m_b to ± 0.3 GeV and take $m_u = 0.2 \pm 0.2 \; GeV$, keeping the above error on $m_b - m_c$. We use the value $\alpha_s(m_b^2) = 0.20 \pm 0.03$, which has been obtained from extrapolating our measured value at $\sqrt{s} \approx M_Z$, $\alpha_s = 0.115 \pm 0.009$ [20], to $Q^2 = m_b^2$. In our treatment, we assume that in accordance with the spectator model the light B-mesons produced at the $\Upsilon(4S)$ have the same semileptonic widths as the heavier B-hadrons which can be produced from the Z^0.

Taking our measured values for τ_B and the B-hadron semileptonic branching ratio [7], we show in Figure 4 the corresponding curve in the $|V_{cb}|$ versus $|V_{ub}|$ plane. The solid line corresponds to the central values, and the dashed lines represent the one standard deviation errors, where the statistical and systematic errors have been added in quadrature. The systematic error has contributions from our measurements and from the uncertainties in the quark masses and α_s. Because of the anti-correlation between m_b and f_c, the factor $(m_b^5 \; f_c)$ in equation (2) varies by only $\pm 12\%$ over the m_b range from 4.65 to 5.25 GeV, if the above error of $\pm 0.02 \; GeV$ on $m_b - m_c$ is maintained. This has to be compared with the $\pm 30\%$ change in m_b^5 alone. However, there is much less of an anti-correlation between m_b and f_u. This explains the widening of the errors in Figure 4 when going from the $|V_{cb}|$ axis to the $|V_{ub}|$ axis.

Measurements of the endpoint of the lepton momentum spectrum from B-meson semileptonic decays [22-23] find the ratio $\frac{|V_{ub}|}{|V_{cb}|}$ to be small. Model-dependent values in the range from 0.1 to 0.2 are obtained. We use the value of $\frac{|V_{ub}|}{|V_{cb}|} = 0.15 \pm 0.10$, which produces the solid straight line shown in Figure 4. The dashed lines again correspond to the estimated error on the ratio. The two solid curves meet at a value

$$|V_{cb}| = 0.046 \pm 0.002\ ^{+0.004}_{-0.003},$$

where the first error is due to our statistical and systematic errors added in quadrature, and the second is due to uncertainties in the theory, including the errors on $\frac{|V_{ub}|}{|V_{cb}|}$, the quark masses[(1)] and α_s. This determination of $|V_{cb}|$ is relatively insensitive to the exact value of $\frac{|V_{ub}|}{|V_{cb}|}$. Varying the ratio from 0.05 to 0.25, changes the value of $|V_{cb}|$ by only $^{+0.001}_{-0.002}$.

Conclusion

We have performed a measurement of the lifetime of hadrons containing b-quarks from a study of inclusive muon and electron events selected from a sample of 115,000 hadronic Z^0 decays. From a fit to the impact parameter distribution of the lepton candidate tracks, the average lifetime of B-hadrons is determined to be:

$$\tau_B = 1.32 \pm 0.08\ (\text{stat.}) \pm 0.09\ (\text{sys.})\ \text{ps}.$$

In the framework of ACCMM model [19], using this measurement and our previously published result on the branching ratio $\text{Br}(B \to \ell\nu X)$, we obtain $|V_{cb}| = 0.046 \pm 0.002\ ^{+0.004}_{-0.003}$.

Acknowledgments

We wish to express our gratitude to the CERN accelerator divisions for the excellent performance of the LEP machine. We acknowledge the effort of all the engineers and technicians who have participated in the construction and maintenance of this experiment. We thank G. Altarelli, B. Stech and P. Zerwas for valuable discussions.

(1) If we use an error of 0.1 GeV on the $m_b - m_c$, it increases the error on $|V_{cb}|$ due to uncertainties in the theory to $^{+0.005}_{-0.004}$

The L3 Collaboration:

B.Adeva,[15] O.Adriani,[13] M.Aguilar-Benitez,[23] H.Akbari,[5] J.Alcaraz,[23] A.Aloisio,[25] B.Alpat,[29] G.Alverson,[9] M.G.Alviggi,[25] G.Ambrosi,[29] Q.An,[16] H.Anderhub,[41] A.L.Anderson,[12] V.P.Andreev,[14] T.Angelov,[12] L.Antonov,[36] D.Antreasyan,[7] P.Arce,[23] A.Arefiev,[24] T.Azemoon,[3] T.Aziz,[8] P.V.K.S.Baba,[16] P.Bagnaia,[32] J.A.Bakken,[31] L.Baksay,[37] R.C.Ball,[3] S.Banerjee,[8] J.Bao,[5] R.Barillère,[15] L.Barone,[32] R.Battiston,[29] A.Bay,[17] U.Becker,[12] F.Behner,[41] J.Behrens,[41] S.Beingessner,[4] Gy.L.Bencze,[10,15] J.Berdugo,[23] P.Berges,[12] B.Bertucci,[29] B.L.Betev,[36] A.Biland,[41] G.M.Bilei,[29] R.Bizzarri,[32] J.J.Blaising,[4] P.Blömeke,[1] B.Blumenfeld,[5] G.J.Bobbink,[2] M.Bocciolini,[13] R.Bock,[1] A.Böhm,[1,15] B.Borgia,[32] D.Bourilkov,[36] M.Bourquin,[17] D.Boutigny,[4] B.Bouwens,[2] J.G.Branson,[33] I.C.Brock,[30] F.Bruyant,[15] C.Buisson,[22] A.Bujak,[38] J.D.Burger,[12] J.P.Burq,[22] J.Busenitz,[37] X.D.Cai,[16] M.Capell,[20] F.Carbonara,[25] P.Cardenal,[15] M.Caria,[29] F.Carminati,[13] A.M.Cartacci,[13] M.Cerrada,[23] F.Cesaroni,[32] Y.H.Chang,[12] U.K.Chaturvedi,[16] M.Chemarin,[22] A.Chen,[43] C.Chen,[6] G.M.Chen,[6] H.F.Chen,[18] H.S.Chen,[6] M.Chen,[12] M.L.Chen,[3] W.Y.Chen,[16] G.Chiefari,[25] C.Y.Chien,[5] M.Chmeissani,[3] C.Civinini,[13] I.Clare,[12] R.Clare,[12] H.O.Cohn,[27] G.Coignet,[4] N.Colino,[15] V.Commichau,[1] G.Conforto,[13] A.Contin,[7,15] F.Crijns,[26] X.Y.Cui,[16] T.S.Dai,[12] R.D'Alessandro,[13] R.de Asmundis,[25] A.Degré,[15,4] K.Deiters,[12] E.Dénes,[10,15] P.Denes,[31] F.DeNotaristefani,[32] M.Dhina,[41] D.DiBitonto,[37] M.Diemoz,[32] H.R.Dimitrov,[36] C.Dionisi,[32] M.T.Dova,[16] E.Drago,[25] T.Driever,[26] D.Duchesneau,[17] P.Duinker,[2] I.Duran,[23] H.El Mamouni,[22] A.Engler,[30] F.J.Eppling,[12] F.C.Erné,[2] P.Extermann,[17] R.Fabbretti,[39] M.Fabre,[41] S.Falciano,[32] Q.Fan,[16] S.J.Fan,[35] O.Fackler,[20] J.Fay,[22] T.Ferguson,[30] G.Fernandez,[23] F.Ferroni,[32,15] H.Fesefeldt,[1] E.Fiandrini,[29] J.Field,[17] F.Filthaut,[26] G.Finocchiaro,[32] P.H.Fisher,[5] G.Forconi,[17] T.Foreman,[2] K.Freudenreich,[41] W.Friebel,[40] M.Fukushima,[12] M.Gailloud,[19] Yu.Galaktionov,[24] E.Gallo,[13] S.N.Ganguli,[8] P.Garcia-Abia,[23] S.S.Gau,[43] D.Gele,[22] S.Gentile,[32] M.Glaubman,[9] S.Goldfarb,[3] Z.F.Gong,[18] E.Gonzalez,[23] A.Gordeev,[24] P.Göttlicher,[1] D.Goujon,[17] G.Gratta,[28] C.Grinnell,[12] M.Gruenewald,[28] M.Guanziroli,[16] J.K.Guo,[35] A.Gurtu,[8] H.R.Gustafson,[3] L.J.Gutay,[38] H.Haan,[1] A.Hasan,[16] D.Hauschildt,[2] C.F.He,[35] T.Hebbeker,[1] M.Hebert,[33] G.Herten,[12] U.Herten,[1] A.Hervé,[15] K.Hilgers,[1] H.Hofer,[41] H.Hoorani,[16] L.S.Hsu,[43] G.Hu,[16] G.Q.Hu,[35] B.Ille,[22] M.M.Ilyas,[16] V.Innocente,[25,15] H.Janssen,[15] S. Jezequel,[4] B.N.Jin,[6] L.W.Jones,[3] A.Kasser,[19] R.A.Khan,[16] Yu.Kamyshkov,[24,27] Y.Karyotakis,[4,15] M.Kaur,[16] S.Khokhar,[16] V.Khoze,[14] M.N.Kienzle-Focacci,[17] W.Kinnison,[21] D.Kirkby,[28] W.Kittel,[26] A.Klimentov,[24] A.C.König,[26] O.Kornadt,[1] V.Koutsenko,[24,12] R.W.Kraemer,[30] T.Kramer,[12] V.R.Krastev,[36] W.Krenz,[1] J.Krizmanic,[5] K.S.Kumar,[11] V.Kumar,[16] A.Kunin,[11,24] V.Lalieu,[17] G.Landi,[13] K.Lanius,[15] D.Lanske,[1] S.Lanzano,[25] P.Lebrun,[22] P.Lecomte,[41] P.Lecoq,[15] P.Le Coultre,[41] D.Lee,[21] I.Leedom,[9] J.M.Le Goff,[15] L.Leistam,[15] R.Leiste,[40] M.Lenti,[13] E.Leonardi,[32] J.Lettry,[41] P.M.Levchenko,[14] X.Leytens,[2] C.Li,[18,16] H.T.Li,[6] J.F.Li,[16] L.Li,[39] P.J.Li,[35] Q.Li,[16] X.G.Li,[6] J.Y.Liao,[35] Z.Y.Lin,[18] F.L.Linde,[15,2] B.Lindemann,[1] D.Linnhofer,[41] R.Liu,[16] Y.Liu,[16] W.Lohmann,[40] E.Longo,[32] Y.S.Lu,[6] J.M.Lubbers,[15] K.Lübelsmeyer,[1] C.Luci,[15] D.Luckey,[7,12] L.Ludovici,[32] L.Luminari,[32] W.G.Ma,[18] M.MacDermott,[41] R.Magahiz,[34] P.K.Malhotra,[8] R.Malik,[16] A.Malinin,[24,4] C.Maña,[23] G.Mantovani,[29] D.N.Mao,[3] Y.F.Mao,[6] M.Maolinbay,[41] P.Marchesini,[41] A.Marchionni,[13] J.P.Martin,[22] L.Martinez-Laso,[15] F.Marzano,[32] G.G.G.Massaro,[2] T.Matsuda,[12] K.Mazumdar,[8] P.McBride,[11] T.McMahon,[38] D.McNally,[41] Th.Meinholz,[1] M.Merk,[26] L.Merola,[25] M.Meschini,[13] W.J.Metzger,[26] Y.Mi,[16] G.B.Mills,[21] Y.Mir,[16] G.Mirabelli,[32] J.Mnich,[1] M.Möller,[1] B.Monteleoni,[13] G.Morand,[17] R.Morand,[4] S.Morganti,[32] N.E.Moulai,[16] R.Mount,[28] S.Müller,[1] E.Nagy,[10] M.Napolitano,[25] H.Newman,[28] C.Neyer,[41] M.A.Niaz,[16] L.Niessen,[1] H.Nowak,[40] D.Pandoulas,[1] M.Pauluzzi,[29] F.Pauss,[41] F.Plasil,[27] G.Passaleva,[13] G.Paternoster,[25] S.Patricelli,[25] Y.J.Pei,[1] D.Perret-Gallix,[4] J.Perrier,[17] A.Pevsner,[5] M.Pieri,[13] P.A.Piroué,[31] V.Plyaskin,[24] M.Pohl,[41] V.Pojidaev,[24] N.Produit,[17] J.M.Qian,[3] K.N.Qureshi,[16] R.Raghavan,[8] G.Rahal-Callot,[41] G.Raven,[2] P.Razis,[37] K.Read,[27] D.Ren,[41] Z.Ren,[16] S.Reucroft,[9] A.Ricker,[1] S.Riemann,[40] O.Rind,[3] C.Rippich,[30] H.A.Rizvi,[16] B.P.Roe,[3] M.Röhner,[1] S.Röhner,[1] L.Romero,[23] J.Rose,[1] S.Rosier-Lees,[4] R.Rosmalen,[26] Ph.Rosselet,[19] A.Rubbia,[12] J.A.Rubio,[15,23] M.Rubio,[15] W.Ruckstuhl,[17] H.Rykaczewski,[41] M.Sachwitz,[40,15] J.Salicio,[15,23] J.M.Salicio,[23] G.Sanders,[21] A.Santocchia,[29] M.S.Sarakinos,[12] G.Sartorelli,[7,16] G.Sauvage,[4] A.Savin,[24] V.Schegelsky,[14] K.Schmiemann,[1] D.Schmitz,[1] P.Schmitz,[1] M.Schneegans,[4] H.Schopper,[42] D.J.Schotanus,[26] S.Shotkin,[12] H.J.Schreiber,[40] R.Schulte,[1] S.Schulte,[1] K.Schultze,[1] J.Schütte,[11] J.Schwenke,[1] G.Schwering,[1] C.Sciacca,[25] I.Scott,[11] R.Sehgal,[16] P.G.Seiler,[39] J.C.Sens,[2] L.Servoli,[29] I.Sheer,[33] D.Z.Shen,[35] V.Shevchenko,[24] S.Shevchenko,[24] X.R.Shi,[28] K.Shmakov,[24] V.Shoutko,[24] E.Shumilov,[24] N.Smirnov,[14] E.Soderstrom,[31] A.Sopczak,[33] C.Spartiotis,[5] T.Spickermann,[1] P.Spillantini,[13] R.Starosta,[1] M.Steuer,[7,12] D.P.Stickland,[31] F.Sticozzi,[12] W.Stoeffl,[20] H.Stone,[17] K.Strauch,[11] B.C.Stringfellow,[38] K.Sudhakar,[8,1] G.Sultanov,[16] R.L.Sumner,[31] L.Z.Sun,[18,16] H.Suter,[41] R.B.Sutton,[30] J.D.Swain,[16] A.A.Syed,[16] X.W.Tang,[6] E.Tarkovsky,[24] L.Taylor,[9] C.Timmermans,[26] Samuel C.C.Ting,[12] S.M.Ting,[12] Y.P.Tong,[43] F.Tonisch,[40] M.Tonutti,[1] S.C.Tonwar,[8] J.Tóth,[10,15] G.Trowitzsch,[40] C.Tully,[28] K.L.Tung,[6] J.Ulbricht,[41] L.Urbán,[10] U.Uwer,[1] E.Valente,[32] R.T.Van de Walle,[26] I.Vetlitsky,[24] G.Viertel,[41] P.Vikas,[16] U.Vikas,[16] M.Vivargent,[4,12] H.Vogel,[30] H.Vogt,[40] G.Von Dardel,[15] I.Vorobiev,[24] A.A.Vorobyov,[14] An.A.Vorobyov,[14] L.Vuilleumier,[19] M.Wadhwa,[16] W.Wallraff,[1] C.R.Wang,[18]

G.H.Wang[30] J.H.Wang[6] Q.F.Wang[11] X.L.Wang[18] Y.F.Wang[13] Z.Wang[16] Z.M.Wang[16,18] A.Weber[1] J.Weber[41] R.Weill[19] T.J.Wenaus[20] J.Wenninger[17] M.White[12] C.Willmott[23] F.Wittgenstein[15] D.Wright[31] R.J.Wu[6] S.L.Wu[16] S.X.Wu[16] Y.G.Wu[6] B.Wysłouch[12] Y.Y.Xie[35] Y.D.Xu[6] Z.Z.Xu[18] Z.L.Xue[35] D.S.Yan[35] X.J.Yan[12] B.Z.Yang[18] C.G.Yang[6] G.Yang[16] K.S.Yang[6] Q.Y.Yang[6] Z.Q.Yang[35] C.H.Ye[16] J.B.Ye[41,18] Q.Ye[16] S.C.Yeh[43] Z.W.Yin[35] J.M.You[16] M.Yzerman[2] C.Zaccardelli[28] P.Zemp[41] M.Zeng[16] Y.Zeng[1] D.H.Zhang[2] Z.P.Zhang[18,16] J.F.Zhou[1] R.Y.Zhu[28] H.L.Zhuang[6] A.Zichichi[7,15,16]

---

1 I. Physikalisches Institut, RWTH, Aachen, Federal Republic of Germany§
III. Physikalisches Institut, RWTH, Aachen, Federal Republic of Germany§
2 National Institute for High Energy Physics, NIKHEF, Amsterdam, The Netherlands
3 University of Michigan, Ann Arbor, Michigan, United States of America
4 Laboratoire de Physique des Particules, LAPP, Annecy, France
5 Johns Hopkins University, Baltimore, Maryland, United States of America
6 Institute of High Energy Physics, IHEP, Beijing, China
7 INFN-Sezione di Bologna, Italy
8 Tata Institute of Fundamental Research, Bombay, India
9 Northeastern University, Boston, Massachusetts, United States of America
10 Central Research Institute for Physics of the Hungarian Academy of Sciences, Budapest, Hungary
11 Harvard University, Cambridge, Massachusetts, United States of America
12 Massachusetts Institute of Technology, Cambridge, Massachusetts, United States of America
13 INFN Sezione di Firenze and University of Firenze, Italy
14 Leningrad Nuclear Physics Institute, Gatchina, Soviet Union
15 European Laboratory for Particle Physics, CERN, Geneva, Switzerland
16 World Laboratory, FBLJA Project, Geneva, Switzerland
17 University of Geneva, Geneva, Switzerland
18 University of Science and Technology of China, Hefei, China
19 University of Lausanne, Lausanne, Switzerland
20 Lawrence Livermore National Laboratory, Livermore, California, United States of America
21 Los Alamos National Laboratory, Los Alamos, New Mexico, United States of America
22 Institut de Physique Nucléaire de Lyon, IN2P3-CNRS/Université Claude Bernard, Villeurbanne, France
23 Centro de Investigaciones Energeticas, Medioambientales y Tecnologicas, CIEMAT, Madrid, Spain
24 Institute of Theoretical and Experimental Physics, ITEP, Moscow, Soviet Union
25 INFN-Sezione di Napoli and University of Naples, Italy
26 University of Nymegen and NIKHEF, Nymegen, The Netherlands
27 Oak Ridge National Laboratory, Oak Ridge, Tennessee, United States of America
28 California Institute of Technology, Pasadena, California, United States of America
29 INFN-Sezione di Perugia and Universitá Degli Studi di Perugia, Perugia, Italy
30 Carnegie Mellon University, Pittsburgh, Pennsylvania, United States of America
31 Princeton University, Princeton, New Jersey, United States of America
32 INFN-Sezione di Roma and University of Roma, "La Sapienza", Italy
33 University of California, San Diego, California, United States of America
34 Union College, Schenectady, New York, United States of America
35 Shanghai Institute of Ceramics, SIC, Shanghai, China
36 Central Laboratory of Automation and Instrumentation, CLANP, Sofia, Bulgaria
37 University of Alabama, Tuscaloosa, Alabama, United States of America
38 Purdue University, West Lafayette, Indiana, United States of America
39 Paul Scherrer Institut, PSI, Würenlingen, Switzerland
40 Institut für Hochenergiephysik, Zeuthen, Federal Republic of Germany§
41 Eidgenössische Technische Hochschule, ETH Zürich Switzerland
42 University of Hamburg, Federal Republic of Germany
43 High Energy Physics Group, Taiwan, China
§ Supported by the German Bundesministerium für Forschung und Technologie

REFERENCES

1. S.L. Glashow, Nucl. Phys. **22** (1961) 579; S. Weinberg, Phys. Rev. Lett. **19** (1967) 1264; A. Salam, Elementary Particle Theory, Ed. N. Svartholm, Stockholm, "Almquist and Wiksell" (1968) 367.
2. N. Cabibbo, Phys. Rev. Lett. **10** (1963) 531;
   M. Kobayashi and K. Maskawa, Prog. Theo. Phys. **49** (1973) 652.
3. JADE Collaboration, W. Bartel *et al.*, Phys. Lett. **B 114** (1982) 71; W. Bartel *et al.*, Z. Phys. **C 31** (1986) 349; J. Hagemann et al., Z. Phys. **C 48** (1990) 401;
   MAC Collaboration, E. Fernandez et al., Phys. Rev. Lett. **51** (1983) 1022; W.W. Ash et al., Phys. Rev. Lett. **58** (1987) 640;
   Mark II Collaboration, N.S. Lockyer et al., Phys. Rev. Lett. **51** (1983) 1316; R.A. Ong et al., Phys. Rev. Lett. **62** (1989) 1236;
   TASSO Collaboration, M. Althoff *et al.*, Phys. Lett. **B 149** (1984) 524; W. Braunschweig et al., Z. Phys. **C 44** (1989) 1;
   HRS Collaboration, J.M. Brom *et al.*, Phys. Lett. **B 195** (1987) 301;
   DELCO Collaboration, D.E. Klem et al., Phys. Rev. **D 37** (1988) 41.
4. ALEPH Collaboration, D. Decamp *et al.*, *Phys. Lett.* **B 257** (1991) 492.
5. L3 Collaboration, B. Adeva *et al.*, *Phys. Lett.* **B 252** (1990) 703.
6. L3 Collaboration, B. Adeva *et al.*, *Phys. Lett.* **B 252** (1990) 713.
7. L3 Collaboration, B. Adeva *et al.*, *Phys. Lett.* **B 261** (1991) 177.
8. CLEO Collaboration, A. Bean *et al.*, Phys. Rev. Lett. **58** (1987) 183; R. Fulton *et al.*, CLNS 90/989, to be published in Phys. Rev. **D**;
   ARGUS Collaboration, H. Albrecht *et al.*, *Phys. Lett.* **B 232** (1989) 554;
   Mark II Collaboration, G. Abrams *et al.*, Phys. Rev. Lett. **64** (1990) 1095.
9. See, for example, J. Kühn and P. Zerwas in "Z Physics at LEP", CERN Report CERN-89-08, eds. G. Altarelli, R. Kleiss and C. Verzegnassi, Vol. I.
10. L3 Collaboration, B. Adeva *et al.*, *Nucl. Inst. and Meth.* **A 289** (1990) 35.
11. O. Adriani *et al.*, *Nucl. Inst. and Meth.* **A 302** (1991) 53.
12. T. Sjöstrand and M. Bengtsson, *Comput. Phys. Commun.* **43** (1987) 367; T. Sjöstrand in "Z Physics at LEP", CERN Report CERN-89-08, Vol. III, p. 143.
13. The L3 detector simulation is based on GEANT Version 3.13, September, 1989. See R. Brun *et al.*, "GEANT 3", CERN DD/EE/84-1 (Revised), September 1987. Hadronic interactions are simulated using the GHEISHA program; see H. Fesefeldt, RWTH Aachen Report PITHA 85/02 (1985).
14. C. Peterson *et al.*, Phys. Rev. **D 27** (1983) 105.
15. For a compilation of experimental results see: J. Chrin, Z. Phys. **C 36** (1987) 163.
16. See J.J. Hernández *et al.*, Review of Particle Properties 1990, *Phys. Lett.* **B 239** (1990) 1, page VII.113.
    We have averaged the PETRA and PEP measurements according to the procedure used by the Particle Data Group.
17. N. Cabibbo and L. Maiani, Phys. Lett. **B 19** (1978) 109; M. Suzuki, Nucl. Phys. **B 145** (1978) 420; A. Ali and E. Pietarinen, Nucl. Phys. **B 145** (1979) 519.

18. C.S. Kim and A.D. Martin, Phys. Lett. **B 225** (1989) 186.
19. G. Altarelli, N. Cabibbo, G. Carbò, L. Maiani and G. Martinelli, Nucl. Phys. **B 208** (1982) 365.
20. L3 Collaboration, B. Adeva *et al.*, *Phys. Lett.* **B 248** (1990) 464;
    B. Adeva *et al.*, *Phys. Lett.* **B 257** (1991) 469.
21. ARGUS Collaboration, H. Albrecht *et al.*, Phys. Lett. **B 249** (1990) 359;
    J.C. Gabriel, Ph.D. Thesis, University of Heidelberg, IHEP-HD/89-1 (1989).
22. CLEO Collaboration, R. Fulton *et al.*, Phys. Rev. Lett. **64** (1990) 16.
23. ARGUS Collaboration, H. Albrecht *et al.*, Phys. Lett. **B 255** (1991) 297.

FIGURE CAPTIONS:

Figure 1 (a) The distribution of the impact parameter divided by the average impact parameter error for hadronic tracks whose flight directions are nearly parallel to the event thrust axis in the $R-\phi$ projection. The curve is the result of the fit over the negative part of the distribution only. The excess on the positive side is due to decays of long lived particles. (b) The distribution of the impact parameter divided by its error for tracks in Bhabha events. The curve is the result of the fit over the entire distribution.

Figure 2 The impact parameter distribution for hadronic background tracks from data. The curve is the result of the fit described in the text.

Figure 3 The impact parameter distribution of the lepton candidate tracks from the data, with the result of the fit superimposed. The contributions from the various lepton categories are shown by the shaded curves.

Figure 4 The contour plot of $|V_{cb}|$ versus $|V_{ub}|$. The solid curved line comes from our measurement of the B-hadron lifetime and the semileptonic branching ratio. The solid straight line comes from the ARGUS/CLEO measurement of $\frac{|V_{ub}|}{|V_{cb}|}$. The dashed lines correspond to one standard deviation errors, including the theoretical uncertainties.

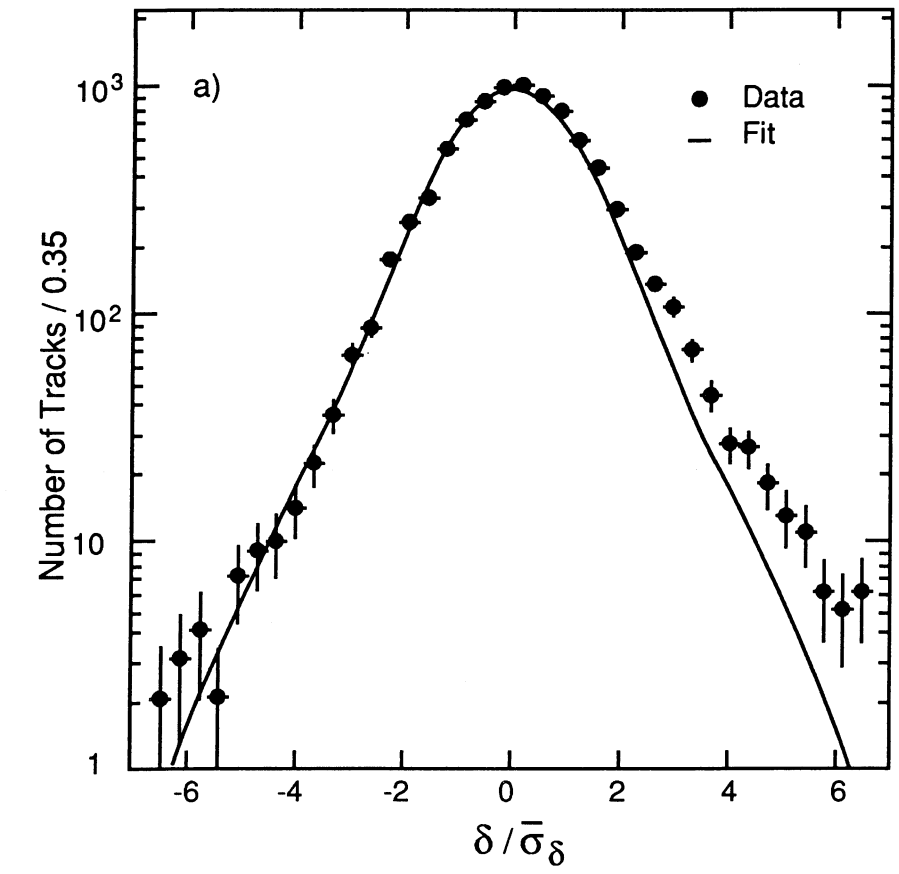
a)
Data
Fit
Number of Tracks / 0.35
10^3
10^2
10
1
-6
-4
-2
0
2
4
6
$\delta / \bar{\sigma}_\delta$

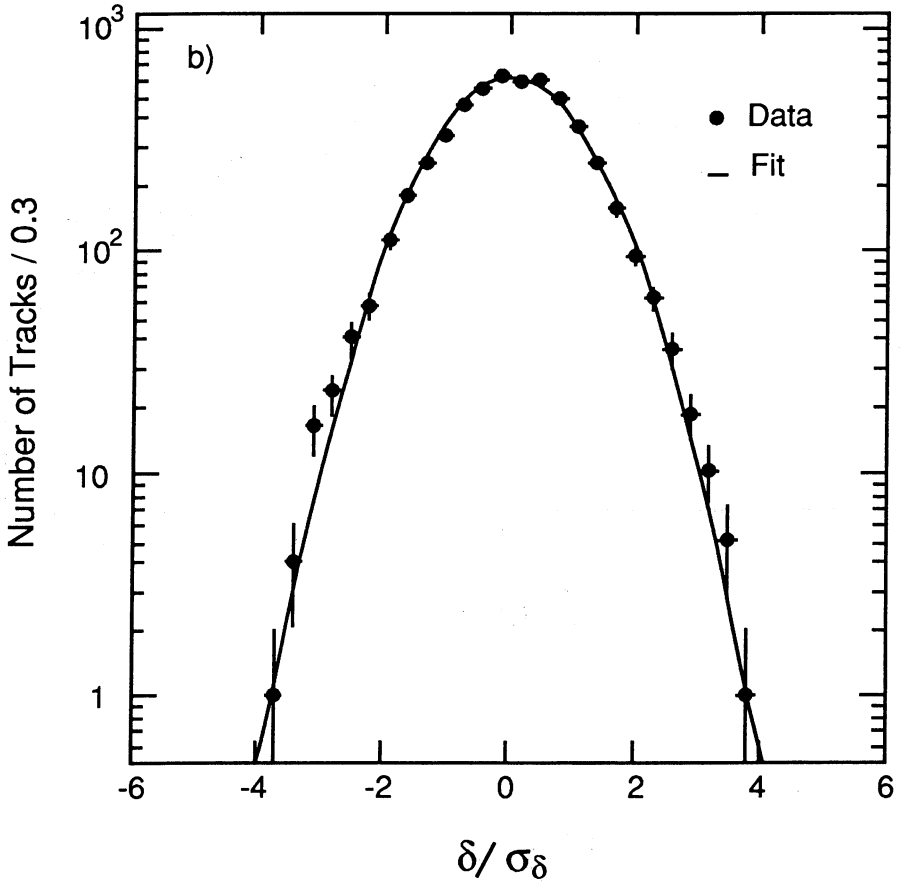
b)
Data
Fit
Number of Tracks / 0.3
10^3
10^2
10
1
-6
-4
-2
0
2
4
6
δ / σ_δ

Fig.1

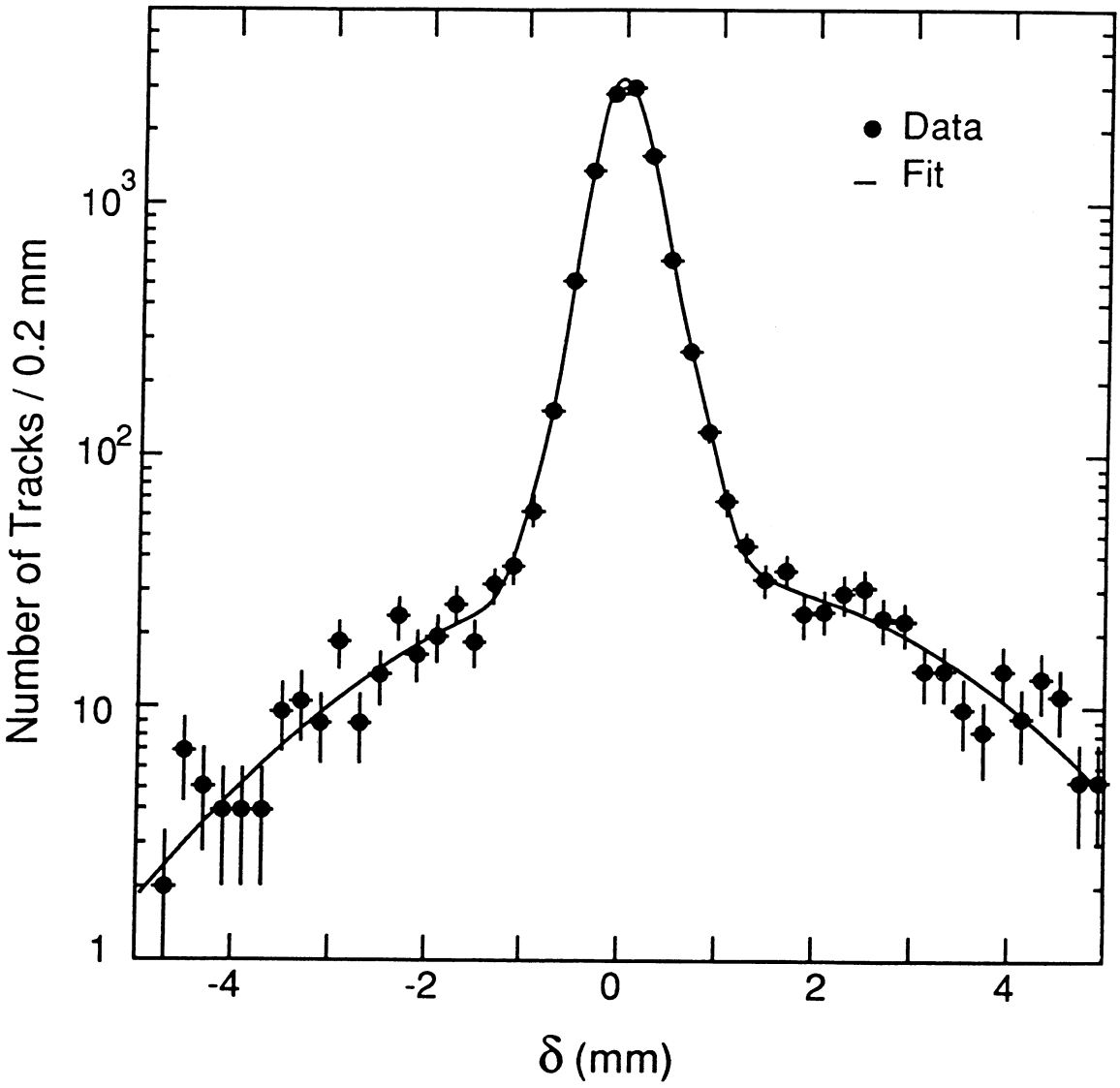

Fig. 2

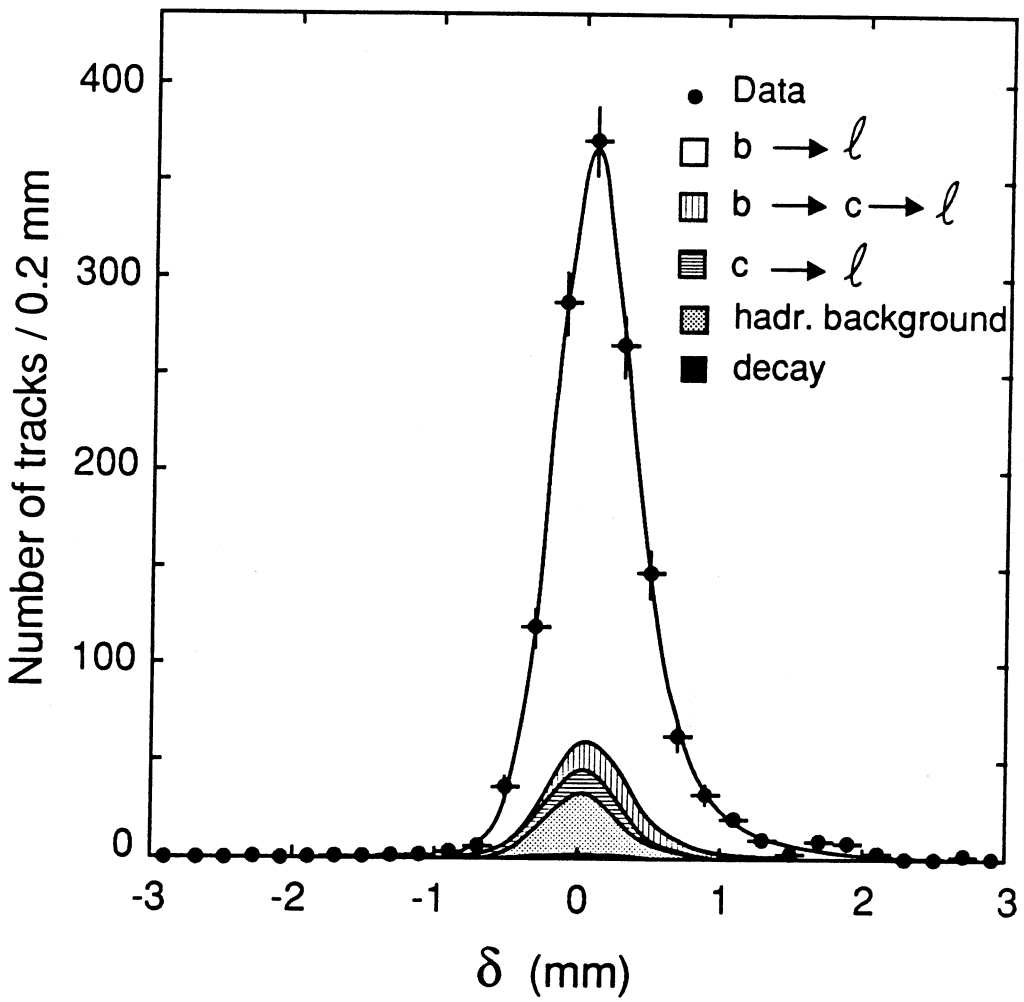
Number of tracks / 0.2 mm
400
300
200
100
0
-3
-2
-1
0
1
2
3
δ (mm)
Data
b → ℓ
b → c → ℓ
c → ℓ
hadr. background
decay

Fig. 3

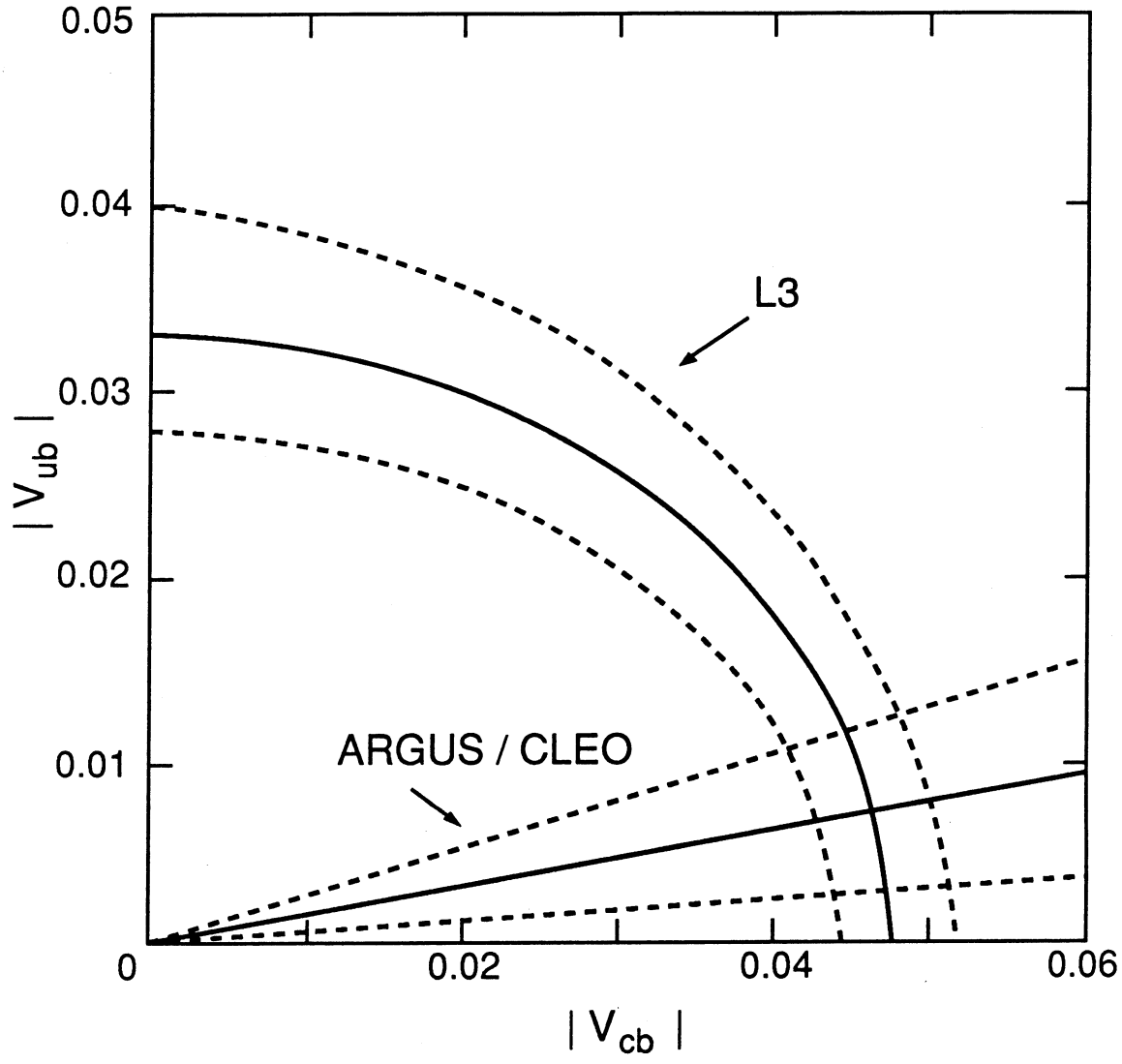

Fig. 4

Imprimé au CERN. Prix: 0.60 Fr.